Biophysical Journal
Article

Biophysical Society

Sticholysin, Sphingomyelin, and Cholesterol: A Closer Look at a Tripartite Interaction

Juan Palacios-Ortega,[1,2] Sara García-Linares,[1] Esperanza Rivera-de-Torre,[1] José G. Gavilanes,[1] Álvaro Martínez-del-Pozo,[1,*] and J. Peter Slotte[2,*]
[1]Departamento de Bioquímica y Biología Molecular, Universidad Complutense, Madrid, Spain and [2]Biochemistry, Faculty of Science and Engineering, Åbo Akademi University, Turku, Finland

ABSTRACT Actinoporins are a group of soluble toxic proteins that bind to membranes containing sphingomyelin (SM) and oligomerize to form pores. Sticholysin II (StnII) is a member of the actinoporin family produced by *Stichodactyla helianthus*. Cholesterol (Chol) is known to enhance the activity of StnII. However, the molecular mechanisms behind this activation have remained obscure, although the activation is not Chol specific but rather sterol specific. To further explore how bilayer lipids affect or are affected by StnII, we have used a multiprobe approach (fluorescent analogs of both Chol and SM) in combination with a series of StnII tryptophan (Trp) mutants to study StnII/bilayer interactions. First, we compared StnII bilayer permeabilization in the presence of Chol or oleoyl-ceramide (OCer). The comparison was done because both Chol and OCer have a 1-hydroxyl, which helps to orient the molecule in the bilayer (although OCer has additional polar functional groups). Both Chol and OCer also have increased affinity for SM, which StnII may recognize. However, our results show that only Chol was able to activate StnII-induced bilayer permeabilization; OCer failed to activate it. To further examine possible Chol/StnII interactions, we measured Förster resonance energy transfer between Trp in StnII and cholestatrienol, a fluorescent analog of Chol. We could show higher Förster resonance energy transfer efficiency between cholestatrienol and Trps in position 100 and 114 of StnII when compared to three other Trp positions further away from the bilayer binding region of StnII. Taken together, our results suggest that StnII was able to attract Chol to its vicinity, maybe by showing affinity for Chol. SM interactions are known to be important for StnII binding to bilayers, and Chol is known to facilitate subsequent permeabilization of the bilayers by StnII. Our results help to better understand the role of these important membrane lipids for the bilayer properties of StnII.

SIGNIFICANCE Sticholysin II (StnII) is a pore-forming toxin that interacts with sphingomyelin in target membranes. Cholesterol (Chol) is known to modulate pore formation. In our study, we examine in detail the molecular interactions between StnII and both pyrene-sphingomyelin and cholestatrienol, a fluorescent Chol analog. We show that both lipids interact with StnII in the bilayer. Using tryptophan mutants of StnII, we also obtained information about which tryptophan residues Chol preferentially interacted with. Our findings provide new, to our knowledge, details on the process of StnII pore formation as influenced by sphingomyelin and Chol.

INTRODUCTION

Pore-forming toxins (PFTs) constitute an important family of membrane-binding proteins. In solution, PFTs are monomeric and behave like globular proteins, with a defined stable conformation. When PFTs encounter membranes with certain lipid compositions, these proteins are capable of forming pores that cause an osmotic shock in the targeted cells (1,2). The proteins undergo a molecular metamorphosis that allows the PFTs not only to bind but also to oligomerize and transform into integral membrane proteins. Therefore, these proteins are also called metamorphic or amphitropic proteins because of this dual behavior (3–6). PFTs can assemble into structures inserted across the bilayer to form pores. This process occurs without covalent modification of the polypeptides involved but also without coupling to any other chemical reaction, although the overall process must be thermodynamically favorable. Taken together, these facts suggest that this family of proteins constitutes a very good model for studying the molecular

Submitted March 15, 2019, and accepted for publication May 10, 2019.

*Correspondence: alvaromp@ucm.es or jpslotte@abo.fi
Sara García-Linares's present address is Cell Biology Department, Harvard Medical School, Boston, Massachusetts.

Editor: Tommy Nylander.
https://doi.org/10.1016/j.bpj.2019.05.010

mechanisms that allow the transition from an aqueous medium to the hydrophobic environment of biological membranes. Sea anemone actinoporins are PFTs that are an optimal system of study, given their structural and functional features (6–8).

Actinoporins constitute multigenic families that have been detected in more than 20 sea anemone species (6,9–11). However, only four species have been characterized in great detail. They are sticholysins I and II (StnI and StnII, respectively) from *Stichodactyla helianthus* (6–8), equinatoxin II from *Actinia equina* (11,12), and fragaceatoxin C (FraC) from *A. fragacea* (13). All show very similar amino-acid sequences and almost identical monomeric and water-soluble three-dimensional structures (14–19), displaying a β-sandwich motif composed of 10−12 β-strands flanked by two α-helices that interact with both sides of the β-sandwich (Fig. 1 *A*) (14–19). One of these helices (α1) is located at the N-terminal end, and it is responsible for the function of the protein. After binding to the membrane, the helix extends to the first 30 residues and inserts into the membrane to form the walls of the pore (Fig. 1 *B*) (14,20–26).

The incorporation of actinoporin into the membrane and the subsequent pore formation depend largely on the composition of the lipid bilayer and physicochemical properties (12,24,27–35). Sphingomyelin (SM) is required (30,36–38), but other conditions in the bilayer membrane (such as the presence of sterols, the coexistence of various phases or domains, lateral packing, fluidity, membrane thickness, and the strength of the interfacial hydrogen bonding network) have a strong influence on the pore-forming ability of the proteins (24,25,30,32–35,39–45). In this context, cholesterol (Chol) greatly influences the pore-forming mechanism considered as a whole (24,25,32,35,44–48). However, the specific role of Chol remains elusive.

It has been shown that in some conditions, the Chol-induced formation of lipid phase boundaries may enhance pore formation by actinoporins (40,41,43,49). However, using 18:1-SM (OSM) bilayers, we have also shown that StnII does not require those phase boundaries for pore formation (24). The results also suggested that as the lateral packing among the SM chains became tighter and the strength of the hydrogen bonds increased, pore formation was hindered (24,34). It has also been observed that fatty acid alcohols (50) and even benzyl alcohol (24) facilitate pore formation by actinoporins. It was proposed that these alcohols interfere with intermolecular hydrogen bonding among SMs, lowering the energy barrier for the diffusion of monomeric actinoporins and oligomerization to constitute a pore (24,34,50). Further confirmation of the hypothesis involving hydrogen bonding arose from the observation that the presence of dihydro-SMs (which lack the *trans* Δ^4 double bond of the long-chain base) (34) strongly impaired toxin binding and pore formation. This effect of establishing a tighter hydrogen bonding network was easily reverted by the presence of Chol. It has been established that many different Chol analogs have a very strong effect on the functionality of actinoporins, facilitating actinoporin-induced membrane permeabilization (24). Given that all the sterols assayed had a 3β-OH group in common, these results seemed to confirm the hypothesis about the strong influence of intermolecular hydrogen bonding in SM bilayers (34) without disregarding the other possibilities of sterols influencing membrane fluidity and SM clustering. Furthermore, Chol appears to affect the SM phosphocholine headgroup orientation and dynamics similarly as seen with glycerophospholipids (51–54), which could facilitate the interaction between actinoporins and SM. Finally, some authors have also suggested that Chol is required for the insertion of the N-terminal α-helix of equinatoxin II into the core of the membrane, enabling the constitution of a fully functional pore (46).

Among all well-known actinoporins, StnII seems to be especially sensitive to the presence of Chol (35). Therefore, in this work, we examined this actinoporin with the aim of shedding further light on our understanding of the role of Chol in pore formation. The results support the need for preferred SM distribution in the membrane for optimal pore formation and the role of Chol in facilitating this distribution. Using a set of tryptophan (Trp) mutants, we also show the specific approach of StnII to Chol in the pore structures.

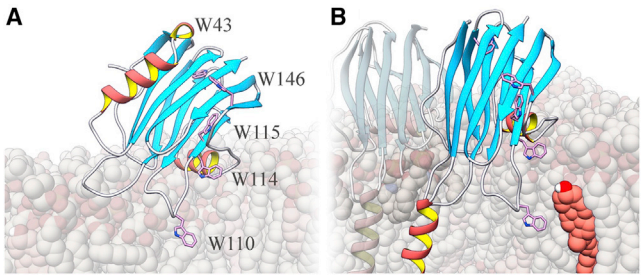

FIGURE 1 Cartoon representation of the expected orientation within the membrane of monomeric StnII (*A*) and its presumed membrane conformation when making an oligomeric pore (*B*). The location and side chains of all its Trp residues are also shown and are in purple. The diagram was constructed using the atomic coordinates deposited in the Protein Data Bank (PDB) for monomeric StnII (PDB: 1GWY) (14) and FraC octameric pores (PDB: 4TSY) (19). A Chol molecule (*salmon*) is highlighted in the membrane. The image was generated with Chimera (93). To see this figure in color, go online.

MATERIALS AND METHODS

Materials

Calcein and Chol were obtained from Sigma-Aldrich (St. Louis, MO). Egg sphingomyelin (eSM), 1,2-dioleoyl-*sn*-glycero-3-phosphocholine (DOPC), 1-palmitoyl-2-oleoyl-*sn*-glycero-3-phosphocholine (POPC), and 1-palmitoyl-2-(7-doxyl)-stearoyl-phosphatidylcholine (7-SLPC) were obtained from Avanti Polar Lipids (Alabaster, AL). Palmitoyl SM (PSM) was isolated from eSM with preparative high-pressure liquid chromatography, as described previously (55). N-C10-pyrene-D-*erythro*-sphingomyelin

(Pyr-SM), oleoyl-ceramide (OCer), and cholestatrienol (CTL) were synthesized and purified in-house using published procedures (56). Wild-type StnII and the different Trp mutants employed were produced in *Escherichia coli* RB791 and purified to homogeneity as described previously (57,58).

Preparation of vesicles

Briefly, vesicles were made by extruding resuspended dried lipid films as described previously (24–26,34). Lipid films were made from a methanol mixture of the desired lipids dried under nitrogen flow. This film was later kept in a vacuum for at least 2 h to ensure complete elimination of the organic solvent. Specific details for each set of experiments are provided in the following sections.

Release of calcein from large unilamellar vesicles

Calcein-entrapped large unilamellar vesicles (LUVs) were prepared from different lipids by extrusion through 200 nm filters at 60°C as previously described (38). The buffer used was Tris buffer (10 mM Tris, 140 mM NaCl (pH 7.4)) containing calcein at 100 mM. The LUVs were used for permeabilization studies within 8 h. The specific compositions of the LUVs are indicated in the corresponding sections or figure legends. The LUV and StnII concentrations during the calcein leakage experiments were 2.5 μM and 20 nM, respectively, unless otherwise indicated. Emission at 550 nm was followed at 23°C as a function of time (the excitation wavelength was 480 nm). Fluorescence emission was measured in a FLUOstar OPTIMA microplate reader (BMG-Labtech, Ortenberg, Germany). The fraction of calcein released was determined based on the maximal calcein release that was induced by LUV disintegration using 10% Triton X-100. To ensure that no spontaneous leakage occurred, the emission was measured for each sample for 3−5 min before the toxin was added. A steady signal level, indicating intact vesicles, was observed for all samples.

Measurement of the excimer/monomer ratio of Pyr-SM in bilayer systems

For measurement of the excimer/monomer (E/M) ratio, POPC:PSM:Pyr-SM (5:3:2), POPC:PSM:Pyr-SM:Chol (5:3:2:1), or POPC:PSM:Pyr-SM:OCer (5:3:2:1) LUVs were prepared. The experiments were carried out at 23°C. The final E/M ratio was determined 10 min after StnII was added. The initial E/M ratio also recorded. The final phospholipid concentration was around 1.0 μM in all experiments shown. The exact value was quantified a posteriori with phosphorous determination, using Rouser's method (59), and was then taken into account to calculate the respective protein/lipid molar ratios. Pyr-SM was excited at 345 nm; the monomer emission was read at 392 nm, whereas the excimer emission was monitored at 480 nm. These, as well as subsequently referred to steady-state fluorescence measurements, were made using a PTI Quanta- Master spectrofluorimeter (Photon Technology International, Birmingham, NJ).

Analysis of CTL fluorescence emission in presence of phase-selective quencher

The steady-state fluorescence emissions were measured essentially as described previously (35,58,60–64). Briefly, 7-SLPC is a phosphatidylcholine analog that contains one bulky doxyl group in the *sn*-2 acyl chain. The doxyl group acts as the collisional quencher for CTL. Because of the bulkiness of the doxyl group, 7-SLPC is largely excluded from the ordered domains in the bilayer and instead is enriched in the liquid-disordered phase of the membrane. For that reason, the membrane compositions used for the samples aimed to monitor the quenched emission intensity (F) were POPC:7-SLPC:PSM:CTL 50:30:20:5 and POPC:7-SLPC:PSM:CTL 30:20:50:5. That way, two different conditions were tested: one in which most CTL would be already protected from the quencher by partitioning into the ordered domain (induced by the high amount of PSM) and one in which the extension of the ordered domain was smaller and CTL would be more accessible to 7-SLPC. To measure the emission in the absence of a quencher, 7-SLPC was replaced by POPC in all samples from which unquenched emission intensity was measured (F_0). All other components were kept constant. The CTL content was kept slightly below 5 mol% to avoid self-quenching (65). Emission at 400 nm was continuously recorded using 310 nm as the excitation wavelength. This value was selected to achieve the maximal excitation of CTL while simultaneously avoiding significant excitation of the Trp residues of the proteins. Any Trp-derived emission was subtracted before the subsequent calculations. The lipid concentration was always around 1 μM in all samples. The exact value was determined a posteriori as described above (59). Different amounts of toxin were added after 100 s of a steady signal level of the CTL emission was recorded. The emission increased and reached a plateau after the toxin was added within less than 100 s in all assays.

StnII-induced protection of CTL from 7-SLPC-induced quenching was determined by obtaining the F/F_0 ratios of each pair of comparable samples at all times. The toxin was added to the F and F_0 samples to compare the effect of StnII on CTL in the presence and absence of 7-SLPC. $\Delta(F/F_0)$ after the toxin was added was calculated to show the decreased exposure of CTL to the quencher in the presence of the actinoporin, as well as the larger increased quantum yield of CTL when 7-SLPC was present in the membrane.

Fluorescence emission from the proteins assayed in the presence of lipid vesicles

The fluorescence emission of the different StnII variants was recorded between 280 and 500 nm. Excitation was set to 260 nm to minimize the direct contributions of CTL in the emission (see the following section). The StnII concentration was 200 nM. Emission spectra were recorded repeatedly after every four additions (two in the final step) of small aliquots of vesicles, each addition giving an increment of 1.3 μM lipid concentration, up to a final lipid concentration of 18.5 μM (92.6 L/P ratio). Equivalent samples, in the absence of the toxin, were used to correct for light scattering contributions to the final emission. The areas used to calculate the relative quantum yield were obtained by numerical integration of the recorded spectra. The lipid composition employed was DOPC:eSM:Chol 1:1:1 to ensure binding of the Trp mutants, given that some show low affinity to vesicles containing a lower percentage of Chol (58).

Measurements of Förster resonance energy transfer from StnII to CTL

The StnII and CTL fluorescence emissions were recorded as described in the previous section. The vesicles had the following composition: DOPC:eSM:sterol (1:1:1), where sterol stands for the total amount of Chol + CTL. The mol% of CTL was increased while the amount of Chol was reduced to keep the sterol mol% constant in the membrane. An equivalent sample, without protein added, was used in all experiments to obtain the background contribution of CTL and light scattering. The Förster resonance energy transfer (FRET) efficiencies were calculated by adjusting the emission of the corresponding toxin in the presence of an equivalent amount of DOPC:eSM:Chol (1:1:1) membranes to that of the same toxin in the presence of membranes that contained CTL. The adjustment was performed by nonlinear least-squares fit of the emission between 325 and 340 nm, which contains only the Trp emission. Subtraction of the fitted spectra from the spectra recorded in the presence of CTL yielded the contribution of CTL to the final emission. A very small peak centered between 300 and 310 nm, corresponding to the unquenched Tyr emission in the presence of

CTL, was also obtained. The energy transfer efficiency was calculated as the factor needed to adjust the unquenched spectra to the quenched spectra.

Preferential distribution of CTL around StnII was determined using the StnII mutant StnII W43/110/114/115F, which contains only a single Trp residue (58), according to a model previously described (66,67). The FRET efficiencies were calculated as specified in the previous paragraph. The fluorescence emission decay was measured using a FluoTime 100 spectrofluorimeter with a TimeHarp260 pico time-correlated single-photon-counting module (PicoQuant, Berlin, Germany). The *trans* parinaric acid was excited with a 297 ± 10 nm light-emitting diode laser source (PLS300; PicoQuant), and the emission was collected through a 435/40 nm single-bandpass filter. Fluorescence decays were recorded at 23°C (temperature controlled by water bath) with constant stirring during measurements. Data were analyzed using FluoFit Pro software obtained from PicoQuant.

According to the location of the Trp146 residue in the three-dimensional structure of StnII, and the expected orientation of the protein in the membrane based on previously obtained oligomeric structures (19), the energy transfer to the *trans* leaflet can be considered negligible. Because of the particular geometric configuration of the StnII-membrane system and the position of Trp146 in the system, we used only the part of the model that describes the FRET to acceptors in the *trans* leaflet to predict the effective FRET from that Trp residue to the CTL molecules in the *cis* leaflet of the membrane. The fundamental reason is that in this model, the part that models the FRET to the *cis* leaflet accounts for the FRET from donors to acceptors in the same diffusion plane, whereas the part that describes the FRET to the *trans* leaflet accounts for the FRET from donors to acceptors that are in a separate, parallel diffusion plane. Briefly, the model is used to calculate what the efficiency of the energy transfer would be for a given donor-acceptor pair that is unlinked and randomly distributed in the membrane according to the Förster distance (R_0) of the pair, the exclusion radius of the acceptor around the donor (R_e), the surface density of the acceptor in the membrane (n), and the distance between the diffusion planes of the donors and the acceptors (h).

The Förster distance of this particular FRET pair was calculated as described (68), using the following expression:

$$R_0 = 0.2108\left(\kappa^2 n^{-4} Q_D J(\lambda)\right)^{1/6}, \quad (1)$$

which yields the Förster distance in Å and where κ^2 is the orientation factor, n is the refractive index, Q_D is the quantum yield of the donor, and $J(\lambda)$ is the overlap integral between the donor's emission spectra and the acceptor's absorption spectra. The orientation factor κ^2 was considered to be 2/3, which represents the dynamic isotropic limit. This value is often used for experiments in membranes (69,70). The refractive index n was set to 1.39, which is the average between n_{water} and the estimated values for n_{membrane}. The use of n_{water} represented an increase of only ~3% in the Förster distance. The quantum yield of Trp146 was assumed to be 0.14, which is the quantum yield of Trp in water (71). Variations of the Q_D value down to 0.1 or up to 0.2 represented only an approximate 6% change compared to the value used for Q_D (0.14) in the final R_0 value. The overlap integral $J(\lambda)$ was calculated as

$$J(\lambda) = \int_0^\infty F_D(\lambda)\varepsilon_A(\lambda)\lambda^4 d\lambda, \quad (2)$$

where F_D is the donor's emission spectra with its area normalized to 1 and ε_A is the acceptor's absorption spectra in $M^{-1}\,cm^{-1}$ units. The R_0 value was 22.9 Å.

The time-dependent probability of remaining unquenched of the donor decay in the presence of unlinked, randomly distributed acceptors in a separate diffusion plane was derived in (72):

$$\rho_{cis'}(t) = exp\left(-2\pi h^2 m \int_0^\omega \left\{ 1 - exp\left[-\left(\frac{R_0}{R_e}\right)^6 \times \left(\frac{t}{\langle\tau\rangle}\right)\alpha^6 \right] \right\} \alpha^{-3} d\alpha \right), \quad (3)$$

where h is the distance between the diffusion planes of the donors and acceptors, m is the surface density of the acceptor, and R_e is the exclusion radius between the donor and the acceptor's projection in the donor diffusion plane. The topological parameter α is defined as $\alpha = h/\sqrt{h^2 + r^2}$, where r is the distance between the donor and the projection of the acceptor in the donor's diffusion plane. The parameter ω is a particular case of α at which $r = R_e$, which is the maximal possible value of α.

According to the published structure of the FraC pore (18), h was considered to be 26–28 Å from the equivalent Trp to Trp146 to the location of Chol molecules in a bilayer. For the exclusion distance R_e, a range of possible values were considered, including the extreme case of 0 Å, which would indicate that the acceptor was located right below the donor. The surface density of CTL (m) in the bilayer was calculated from its mole fraction in the bilayer using areas per lipid molecule of 48 $Å^2$ for POPC in the presence of 0.3 mol% of sterol (73), 47.4 $Å^2$ for PSM (74), and 37.7 $Å^2$ for CTL (67,73).

The decay of the donor in the presence of the acceptor in the *cis* leaflet is given by $I_{DA}(t) = I_D(t)\rho_{cis'}(t)$. The theoretical FRET efficiency is then calculated as

$$E = 1 - \frac{\int_0^\infty I_D(t)\rho_{cis'}(t)dt}{\int_0^\infty I_D(t)dt}, \quad (4)$$

where $I_D(t)$ represents the decay of the donor in the absence of the acceptor. For randomly distributed donors and acceptors, experimental results would lie on the theoretically predicted line. However, if the acceptor is preferentially distributed near the donor, the observed FRET efficiencies would be greater than the theoretical values as if the R_0 were larger, although what actually happens is that the average donor-acceptor distance is smaller than expected for a random distribution. The same reasoning, with opposite effects, is valid for acceptors that are excluded from the vicinity of the donor.

RESULTS

StnII causes similar Pyr-SM declustering regardless of the presence of Chol or OCer

Clustering of pyrene-labeled lipids between different bilayer domains can be studied by measuring the pyrene E/M emission ratio (75–77). Therefore, Pyr-SM was employed to study the effect of StnII on SM cluster dispersion. In addition to using Chol, we opted to also test OCer for the following reasons. OCer is a lipid that, like Chol, is prone to interact with SM. The unsaturation in the acyl chain of this ceramide species prevents it, however, from forming gel phases in the range of temperatures that were used. This is particularly important because, as has been shown before (45), gel phase formation hinders the activity of StnII. OCer displays two molecular features that are of interest for the work presented herein: first, its mentioned ability

to interact with SM without forming gel phases (24,34), and second, the presence of its interfacial hydroxyl group. This (C1)OH is in a similar location relative to the membrane to that of Chol. By comparing the effect of OCer and Chol on StnII behavior, we aimed to ascertain whether either of these characteristics are the ones that influence Chol's property as a StnII activator.

It is known that SM molecules tend to cluster in equimolecular mixtures of POPC (78). As shown in Fig. 2, a high E/M ratio value of 3.45 was obtained in these conditions. The inclusion of OCer or Chol in the vesicles resulted in a considerable reduction in the ratio. The values decreased to 2.78 and 2.38 in the vesicles containing 9.1 mol% of OCer or Chol, respectively (Fig. 2). This result shows that both lipids can intercalate among SM molecules, thus diminishing the direct Pyr-Pyr interactions that result in excimer emission. Accordingly, Chol would be a slightly better intercalator than OCer. This result might also be related to the documented (24,25,32,35,43–49) improvement in StnII activity observed in the presence of Chol.

Addition of StnII also resulted in a further decrease in the E/M ratio, although the decrease followed a protein concentration dependence that was practically independent of the presence of OCer or Chol (Fig. 2). Thus, the StnII-induced reduction in Pyr-Pyr contacts could be caused by StnII itself intercalating some residue between the Pyr groups or by StnII-induced intercalation of other lipids among the Pyr-SMs.

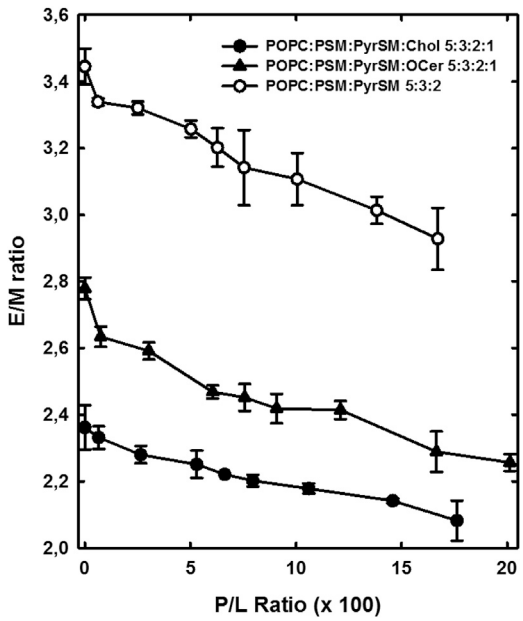

FIGURE 2 The Pyr-SM E/M ratio as a function of various StnII concentrations. POPC:PSM:Pyr-SM (5:3:2) (○), POPC:PSM:Pyr-SM:OCer (5:3:2:1) (▲), or POPC:PSM:Pyr-SM:Chol (5:3:2:1) (●) LUVs were employed at a final phospholipid concentration of 1 μM (approximate). The final stable E/M ratio was determined at 23°C, 10 min after the addition of the protein. Pyr-SM was excited at 345 nm; the monomer emission was read at 392 nm, and the excimer emission was monitored at 480 nm. Each value is the average mean ± standard error (SE) (n = 2–3).

Chol is a better enhancer of the activity of StnII than OCer

One of the questions that remains unsolved is whether the Chol-enhancing effect of actinoporin action (24,25,32,35,43–49) is a major consequence of the formation of lipid boundaries within the membrane because of the existence of liquid-ordered (L_o) phases or whether it is the result of other effects of Chol. As stated in the Introduction, it has been shown that lateral packing or clustering of SM is important (as also observed in this work; see Fig. 2) and how distortion of the SM hydrogen bonding network has a profound effect on actinoporin activity (24,34,50). To further test this hypothesis, calcein leakage experiments were carried out. We first used DOPC:SM (80:20) LUVs that contained increasing amounts of either Chol or OCer. Both lipids showed a high affinity for SM, intercalating between SM molecules (Fig. 2), and contained a hydroxyl group whose location at the bilayer/aqueous interphase was similar. It is possible that this interfacial hydroxyl can distort the intermolecular hydrogen bonding network of SMs. OCer, however, did not participate in creating defined liquid-ordered domains with SM as Chol can do (79).

As seen in Fig. 3, Chol greatly increased the release rates for calcein even when present at a low percentage. The effective Chol concentration was probably below the threshold needed for the formation of Chol-induced lipid domains (80). However, OCer failed to activate StnII-induced release of calcein (Fig. 3). The effect of Chol was noticeably more pronounced, perhaps because of its

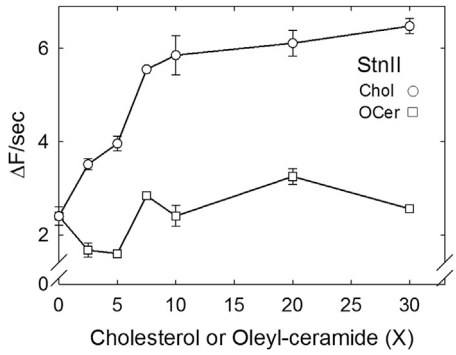

FIGURE 3 Maximal rates of StnII induced the release of calcein entrapped in DOPC:SM:X (80:20:X) LUVs, containing different amounts (X) of Chol (○) or OCer (□). The StnII concentration was 10 nM in all experiments, and the protein/lipid molar ratio was maintained at 0.09. Calcein-entrapped vesicles were prepared via extrusion, and release was measured at 23°C. All intensities were normalized. The maximal rate of release (ΔF/s was measured as the initial slope of the leakage curves) was measured by comparison with protein-free samples to which Triton X-100 was added to a final concentration of 0.05% v/v to induce LUV disintegration. The results shown are representative of three independent experiments. Each value is the average mean ± SE (n = 3).

particular structure. Interestingly, at 20 mol% Chol, at which the L_d/S_o phase boundary appears, no further increase in Chol-promoted activation was observed. In both cases, these enhancing effects became stable when the proportions employed were 80:20:7.5, that is, for an amount of Chol slightly smaller than ~7 mol%.

StnII changes the CTL microenvironment

Partitioning of a fluorescent probe between fluid and ordered membrane domains can be determined by using a phase-selective quencher (81). With the aim of studying the effect of StnII on membranes that contain SM and Chol, the fluorescent Chol analog CTL was used as a probe (56,65,82), whereas 7-SLPC was chosen as a phase-selective collisional quencher (Fig. 4). The gel-to-liquid phase transition temperature of 7-SLPC has been determined to be ~8°C (83), and thus, this lipid is in the fluid state at 23°C, the temperature at which the experiments were carried out.

POPC:7-SLPC:PSM:CTL (50:30:20:5) vesicles were employed. At this concentration, CTL is not self-quenched. The sterol content was similar to that showing the maximal enhancement in the release rate of calcein in Fig. 3. In this situation, the recorded initial F/F_0 value was 0.27, revealing that most of the CTL was accessible to the quencher (Fig. S1). The addition of StnII induced an increase in the observed F/F_0 value that revealed how StnII exerted a considerable quenching-protection effect on CTL (Fig. 4). Given that the quencher is known to partition preferentially into the fluid phase, these results can be interpreted as the protein reducing CTL contacts with fluid-phase lipids, making CTL less available for 7-SLPC quenching. If StnII binds CTL, it could also be that the bound CTL is protected by the protein and not only that StnII redistributes CTL more to the SM phase. In the absence of 7-SLPC, StnII caused an increase in the CTL quantum yield, most probably by shielding it from water. Overall, it seems that the most probable interpretation is that when 7-SLPC is present, StnII produces a change in the lipids surrounding CTL. When the vesicles employed were POPC:7-SLPC:PSM:CTL (30:20:50:5), in which the SM proportion was much higher (nearly ~50 mol%), this effect was greatly reduced (Fig. 4). Higher PSM content decreases the extent of the phase boundary as a consequence of the larger domains. This is reflected in the initial F/F_0 value (0.78), implying CTL is already shielded from the quencher. The interaction of StnII with the membrane is expected to be essentially the same, in terms of activity and affinity, to that in the previous scenario. In this new situation, CTL protection from the quencher was modest (Fig. 4). This expected result confirmed that in SM-rich bilayers, most CTL is not accessible to 7-SLPC because of the preferential partitioning of CTL into the ordered phase and its preferred interaction with PSM.

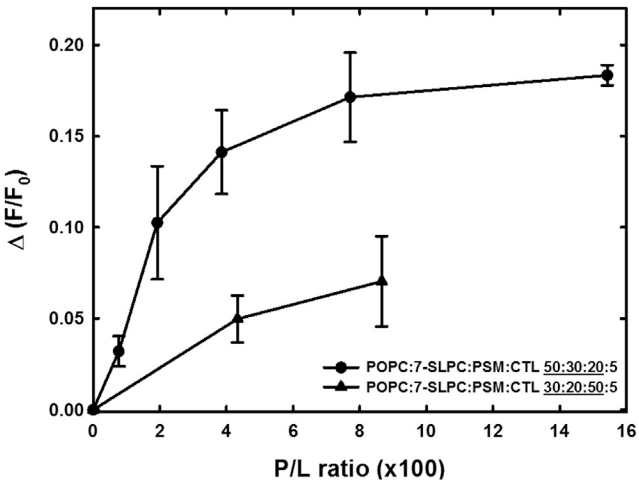

FIGURE 4 Analysis of the effect of StnII on the CTL relative quantum yield embedded in POPC:7-SLPC:PSM:CTL (50:30:20:5) (●) or (30:20:50:5) (▲) vesicles at different protein/lipid (P/L) molar ratios. This relative quantum yield change was expressed as the change in the fluorescence emission for each StnII concentration used. The excitation wavelength employed was 310 nm. CTL emission was recorded at 410 nm. All measurements were conducted at 23°C. Each value is the average mean ± SE ($n = 2$).

StnII Trp side chains move to a more hydrophobic environment in the presence of vesicles that contain SM and Chol

To study the presumed closeness between StnII and Chol in membranes that contain SM, the FRET between Trp residues in StnII and CTL was the chosen approach. Energy transfer suggests the establishment of very close StnII-Chol interactions. A collection of Trp-to-Phe mutants, which had been characterized in a previous work (58), were available. The protein variants assayed were the wild-type protein (StnII WT), a single mutant (W43F), two double mutants (W43/110F and W43/114F), one triple mutant (W43/110/114F), and one quadruple variant (W43/110/114/115F) (Fig. 1). This quadruple mutant contained only a single Trp, specifically W146.

First, titration of the different StnII variants with increasing amounts of DOPC:eSM:Chol (1:1:1) LUVs was performed (Fig. 5). DOPC was used instead of POPC because the Trp mutants employed had already been characterized in this system, in which we already knew that they displayed a considerable membrane binding (53). This vesicle composition, containing a large proportion of Chol, was indeed needed because of the low affinity of some of the Trp mutants employed for the membranes that contained low amounts of this sterol (58). In all experiments, the fluorescence emission spectra of the proteins displayed a considerable increase in the quantum yield (Fig. 5, *right column*), a blue shift in the emission maximum, and a reduction in the spectral width (Fig. S2). The first two are expected features of Trp side chains

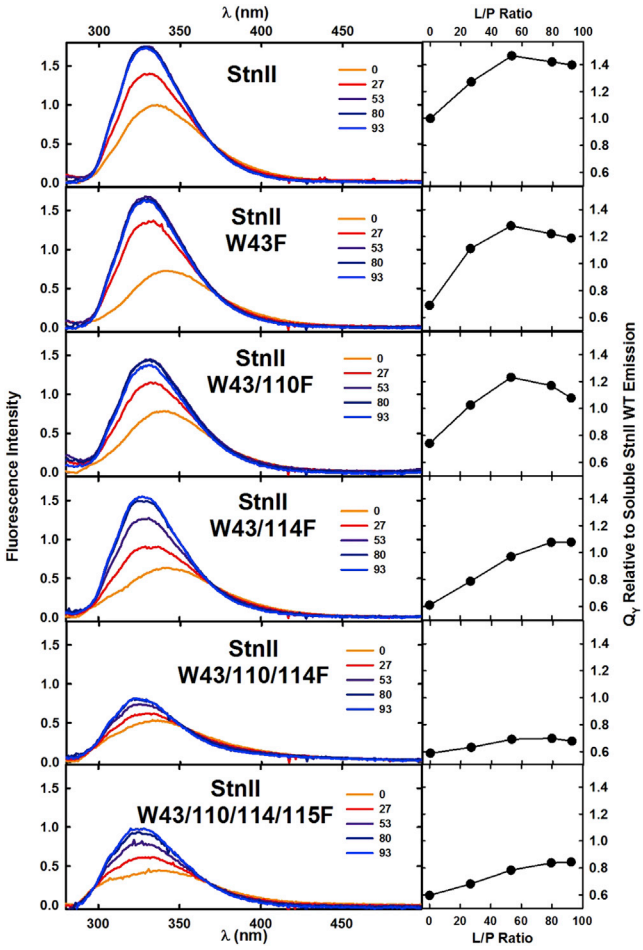

FIGURE 5 Fluorescence spectra of StnII WT and its different mutants used titrated with DOPC:eSM:Chol (1:1:1) LUVs. The panels at the right represent the relative quantum yield change as a function of the L/P ratio, using the quantum yield of StnII WT free in solution as reference. The excitation wavelength employed was 260 nm. The spectra were recorded at 25°C. The protein concentration was 200 nM in all experiments shown. Fluorescence intensities were normalized to 1.0 for the maximal emission of StnII WT in buffer, in the absence of vesicles. To see this figure in color, go online.

entering a more hydrophobic microenvironment. The third one can be also explained as Trp residues changing from varied environments to a relatively equal, nonpolar environment. The observed increases in the quantum yield suggest that W110 and W114 were responsible for most of the effects observed. Representation of the relative change in the quantum yield as a function of the lipid/protein molar ratio (L/P ratio) showed how saturation was reached at similar L/P ratios (Fig. 5, *right column*) for StnII WT, W43F, and W43/110F mutants. W43/114F reaching saturation at a higher L/P ratio confirmed, as previously described using isothermal titration calorimetry, that W114 is more important for membrane affinity than W110, although W110 is more exposed to the aqueous phase than W114 when the protein is in solution (58). Accordingly, substitution of both Trp residues by Phe produced variants in which the quantum yield was barely increased (see the results for the triple and quadruple Trp mutants in Fig. 5).

CTL is located near StnII Trp residues 110 and 114

The same StnII variants were titrated with other vesicles at the DOPC:eSM:sterol ratio of 1:1:1 but contained 5 mol% CTL. Nonradiative energy transfer from the Trp side chains to this fluorescent version of Chol was clearly observed (Fig. 6). This result suggested that the indole moiety of these amino acids was in close proximity to CTL molecules to be able to produce the observed effect. Again, the FRET was especially relevant for proteins containing Trp residues 110 and 114 (Fig. 6). Representation of the CTL emission originating from the FRET as a function of the L/P ratio led to the same conclusion and further confirmed the previous observation that saturation was reached at very similar lipid concentrations in all experiments (Fig. S3). Again, substitution of Trp110 and Trp114 for Phe rendered proteins that were capable of less energy transfer to CTL (W43/110/114F and W43/110/114/115F in Figs. 6 and 7).

There is preferential distribution of Chol near StnII

Among all 20 canonic protein amino acids, Trp stands out because of the properties of its side chain. The indole ring is not only the bulkiest side-chain group but also provides the potential to interact with various molecules. It is a rigid planar ring that can establish a wide variety of very different interactions with other groups, including hydrogen bonding, dipolar or cation-π interactions, and hydrophobic effects (64,84–87). Given that Chol also has a complex and hydrophobic rigid ring structure, it could interact with the indole ring of Trp.

To resolve whether Chol is preferentially distributed near StnII, an approach previously described by Holt et al. (67) was used. A mutant containing only one Trp, the StnII-W43/110/114/115F mutant, was used to avoid complications with the application of the model employed. This single Trp variant appeared to be one of the few soluble StnII mutants containing only one Trp residue. Furthermore, this remaining Trp did not seem to be directly involved in protein-lipid interactions, as shown in Fig. 5 and by García-Linares et al. (58). Instead, Trp146 appears to be needed for protein-protein interactions that lead to oligomerization and pore formation (Fig. 1) (19,58). The increase in the quantum yield observed for this quadruple Trp-to-Phe mutant is interpreted as the side chain of Trp146 entering a hydrophobic cavity in the neighboring actinoporin monomer in the final pore structure (19).

According to the model used (67), if the acceptor (CTL) is randomly distributed around the donor, the experimental FRET efficiencies are located on the theoretical FRET efficiency curve. If the acceptor is preferentially distributed

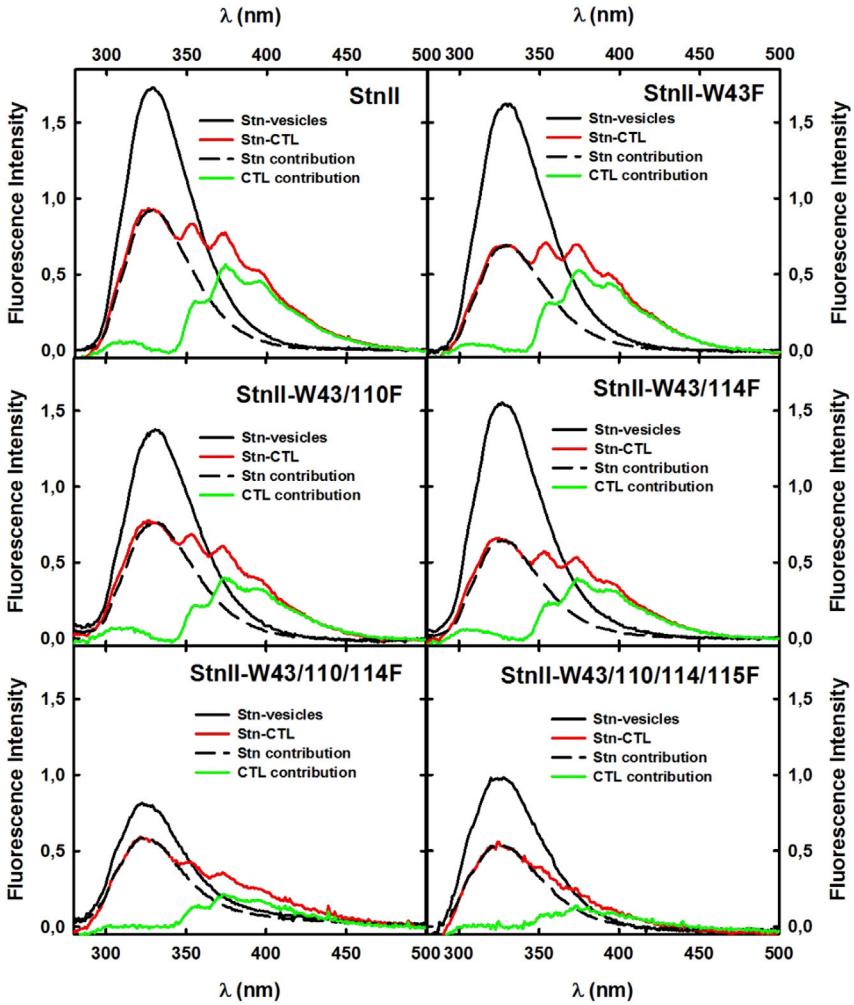

FIGURE 6 Fluorescence emission spectra of StnII WT and the Trp mutants studied in the absence or presence of DOPC:eSM:Chol:CTL (33:33:28:5) at a saturating L/P ratio of 93 (see Fig. 5). The excitation wavelength employed was 260 nm, and the spectra were recorded at 25°C. The protein concentration was 200 nM in all experiments shown. Fluorescence intensities were normalized to 1.0 for the maximal emission of StnII WT in buffer in the absence of vesicles. To see this figure in color, go online.

near the donor, the experimental values are located above it because of the reduced average distance (which still must be larger than the exclusion distance). The plot representing the empirically determined energy transfer efficiencies at several different surface densities of CTL (*dots* in Fig. 7) versus the theoretical curves for the expected energy transfer (*lines* in Fig. 7) shows that the experimental data were higher than the calculated efficiencies. This conclusion is supported even considering that CTL can be located right below the donor ($R_e = 0$ Å) while also at the shortest estimated possible distance from Trp146.

This result indicates that CTL is preferentially distributed near StnII. Given that the sterol effect on this protein's activity has been shown to be largely independent of the sterol structure (24), this result can also be extrapolated to Chol.

DISCUSSION

The presence of Chol in bilayer membranes affects several membrane properties that can influence the function and distribution of membrane proteins. Chol has an ordering effect on acyl chains of surrounding phospho- and sphingolipids, which results in more condensed bilayers. It is also well known that Chol displays high affinity for SM when embedded in a biological membrane (54,88). This observation explains the existence of SM- and Chol-rich L_o domains. Accordingly, it has been proposed that the presence of lipid domains in the membrane could explain the observed effects of Chol on actinoporin activity. The results presented here show that StnII-induced activation of the calcein release phenomenon starts to be observable at a mol% of Chol below the minimal amount needed for SM and Chol to arrange into distinct lipid domains (80) (Fig. 3). Furthermore, qualitatively speaking, OCer, another good SM intercalator (Fig. 2), does not show such behavior (Fig. 3).

SMs form extensive intramolecular hydrogen bonds (from the 3OH of the long-chain base to phosphate oxygens of the headgroup), but also intermolecular hydrogen bonding involving the NH of the long-chain base is important for SM (and sphingolipid) properties in membrane environments (89). Similar hydrogen bonds cannot be established among glycerophospholipids. Hydrogen bonding

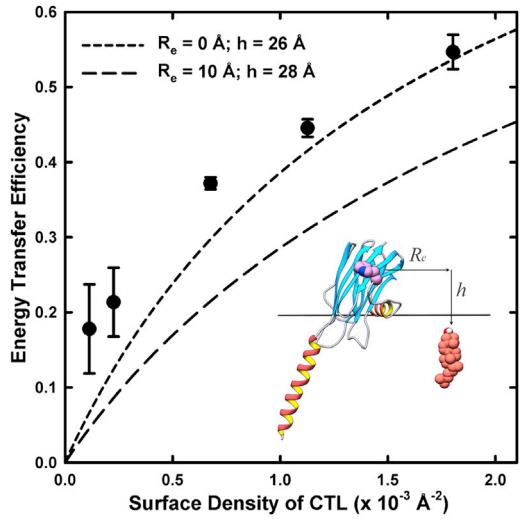

FIGURE 7 Theoretically calculated FRET efficiency curves for StnII Trp146 side chains to CTL. The R_0 of the FRET pair is 22.9 Å. The experimental values (*dots*) were calculated from fluorescence spectra of StnII W43/110/114/115F in vesicles composed of DOPC:eSM:sterol 1:1:1, with increasing amounts of CTL: 0.5, 1, 3, 5, and 8 mol%. FRET efficiencies were calculated for an L/P ratio of 93. Theoretical FRET values were calculated assuming a model based on the random distribution of the donor (StnII W43/110/114/115F) and the acceptor (CTL) and taking into account only the transfer to the *cis* leaflet (67). The distance between diffusion planes was considered to be 26–28 Å, based on the location of the equivalent Trp residue in the crystalline structure of the FraC pore (PDB: 4TSY) (19). Extreme conditions for interplanar and exclusion distances were simulated ($R_e = 0$, $h = 26$ Å; *short dashed line*), showing that even then, the experimental values (given as mean + standard error of $n = 3$) were above the predictions for random distribution. As an example, other conditions were also simulated ($R_e = 10$, $h = 28$ Å; *long dashed line*). To see this figure in color, go online.

involving SM has been also shown to markedly stabilize interactions with both Chol and ceramide in fully hydrated bilayers (90). We have demonstrated before (24,45) that the existence of a fluid phase is important for the formation of pores by actinoporins. These results, combined with the use of benzyl alcohol and several different sterols, suggested that these compounds enhance StnII action by modifying the SM interfacial hydrogen bonding network (24,34). This effect was interpreted as leading to a more favorable distribution of SM molecules in the membrane and to easier availability to StnII molecules.

Chol and OCer share an interfacial hydroxyl group as a common feature. Its location enables hydrogen bonding with other lipid headgroups, especially with SM. Thus, both OCer and Chol could potentially interfere with the hydrogen bonding networks formed by SMs, although they are likely to disturb the network differently because OCer has more possibilities to form hydrogen bonds compared to Chol. Another consequence of the arrangement of Chol in the membrane is that membrane domains with increased Chol content (i.e., lipid rafts), can have an increased bilayer thickness. This agrees with the observation that Chol is not only required for complete membrane penetration by actinoporins (46) but also for optimizing membrane thickness for StnII action (25). Our results here show, however, that the presence of an interfacial (C1)OH group is not enough to explain the observed effect of Chol-enhancing StnII activity because OCer, with a similar (C1)OH group does not induce a comparable effect. Because OCer has an unsaturated acyl chain, its molecular volume requirement in bilayers is larger than that of Chol. This implies that lateral packing is denser in Chol/SM domains or small clusters (condensing effect) than it is in OCer/SM domains or clusters. Such differences in lateral packing in the SM-rich domains could affect SM headgroup orientation differently and explain why Chol does and OCer does not activate StnII-induced bilayer permeabilization.

It has been shown that mixtures in which 1,2-dimyristoyl-*sn*-glycero-3-phosphocholine is in molar excess over PSM hinder SM to participate efficiently in the StnII-induced pore formation process (24). Considering that dimyristoyl phosphatidylcholine displays near-ideal miscibility with PSM, this observation was interpreted as StnII needing small clusters of SM to oligomerize and form pores. Building on previous work in which we used Pyr-SM to show that StnII causes SM declustering (24), in this work, we used Pyr-SM to test the effect of the presence of Chol or OCer on SM distribution. The results showed that both Chol and OCer could decluster Pyr-SM similarly, although Chol was slightly more efficient. However, based on the Pyr-SM results, it is difficult to argue whether or not SM headgroup orientation or presentation to the StnII was markedly different during Chol-induced SM declustering compared to OCer-induced SM declustering.

A question can be raised whether Chol-induced lipid rearrangement is sensed by the toxin or induced by it. According to the results shown in Fig. 4, the answer to this question seems to be, at least partially, the latter. StnII binding to the membrane resulted in a reduction in the contact of CTL with fluid-phase lipids, which could be caused by the effective removal of CTL molecules from the fluid phase. Presumably, lipids from the more ordered domain, essentially SM (Fig. 4), would then surround CTL. However, in the presence of a large amount of SM, the preferential partitioning of Chol (in this instance, CTL) into the ordered phase was more noticeable, as seen in the high initial F/F_0 values. Therefore, the observable effect in the CTL distribution after the addition of the toxin was small, indicating that the SM-CTL arrangement was better for StnII action in this case. These results suggest that StnII induced a rearrangement of CTL distribution in the membrane, probably by recruiting CTL to the pore structure or to the close vicinity of membrane-bound StnII.

Most actinoporins contain five conserved Trp residues (Fig. 1). At least two of them (W110 and W114 in StnII) have been shown to be part of an exposed and conserved cluster of aromatic residues that are implied in the interaction with membranes (8,19,37,58,91,92). Our results

showed that these two amino acids not only contribute to membrane binding but also insert into the hydrophobic region of the bilayer (Fig. 5). This result is also in strong agreement with the previous hypothesis that the key role of membrane recognition assigned to the actinoporin's tryptophan represented by W110 and W114 of StnII is based more on its participation in maintaining a hydrophobic effect than on the onset of interactions with specific SM chemical groups (58). The observed FRET indicates that CTL is located near W110 and W114. It could be argued, however, that the FRET with CTL does not originate from a specific interaction but only from the abundance of CTL available at a short distance from the Trp indole side chains. It has been shown how Chol remains homogeneously distributed in the membrane in the presence of some Trp-flanked transmembrane peptides and how the dynamics and orientation of neither Chol nor Trp located at the bilayer interface were influenced by the presence of the other molecule (67). However, when we used a very similar approach, we observed the opposite effect (Fig. 7). The FRET efficiency from W146 of StnII appeared above the theoretical curves, indicating that the acceptor (CTL) was preferentially distributed close to the donor (StnII). Because the distance measurements were based on a model obtained with detergents (19), we considered the interplanar distance to range from 26 to 28 Å. CTL preferential distribution near StnII held true even for the simulation of the limiting conditions, at which we assume that CTL can diffuse freely below W146 ($R_e = 0$ Å) and the interplanar distance, h, is 26 Å. If the StnII pores contain lipids, then an exclusion distance should be considered because lipids forming part of the pore would have a much lower diffusion rate and hinder diffusion of the remaining lipids near the complex. In that case, the theoretical FRET efficiency would be lower (Fig. 7, *long dashed lines*). The comparatively large FRET efficiencies would then support CTL being part of such a lipid-protein complex. The model, regardless of the distance constraints that are used, overestimates the expected FRET efficiencies. It considers the FRET from the donor to anywhere around it, which, in the particular case of StnII pores, is not correct because the pores themselves create a volume that cannot be transited by lipids.

CONCLUSIONS

Taken together, our results have shown that Chol and OCer behaved differently with regard to StnII-induced bilayer permeabilization. We speculate that headgroup orientation in SM clusters was different in the presence of Chol and OCer, and that the Chol-induced orientation was preferred by StnII. Because StnII activation in bilayers is markedly affected by hydrogen bonding (90), it is also possible that Chol and OCer rearranged SM hydrogen bonding differently, which in turn affected StnII-induced bilayer permeabilization. Such rearrangements of SM hydrogen bonding may also have affected SM headgroup orientation. Using FRET between Trp in StnII and the fluorescent Chol analog CTL in the bilayer, we were able to show that CTL displayed the closest proximity to Trp in positions 100 and 114 of StnII. These two Trp positions are in the membrane-binding region of StnII (Fig. 1), which makes perfect sense and further supports how StnIIs are oriented with regard to the bilayer.

SUPPORTING MATERIAL

Supporting Material can be found online at https://doi.org/10.1016/j.bpj.2019.05.010.

AUTHOR CONTRIBUTIONS

J.P.-O., S.G.-L., and E.R.-d.-T. conducted the experiments. All authors contributed to conceiving and designing the experiments, analyzing the results, and writing the manuscript.

ACKNOWLEDGMENTS

This research was supported by the Sigrid Juselius Foundation, the Jane and Aatos Erkko Foundation, and the Magnus Ehrnrooth Foundation (to J.P.S.), and by grants from UCM-Banco Santander grants PR41/17-21012 and PR75/18-21561 (to A.M.-d.-P.). J.P.-O. has a funded doctoral student position from ISB/ÅA. FPU and UCM-Banco Santander fellowships were granted to S.G.-L. and E.R.-d.-T., respectively.

REFERENCES

1. Parker, M. W., and S. C. Feil. 2005. Pore-forming protein toxins: from structure to function. *Prog. Biophys. Mol. Biol.* 88:91–142.
2. Gilbert, R. J., M. Dalla Serra, …, G. Anderluh. 2014. Membrane pore formation at protein-lipid interfaces. *Trends Biochem. Sci.* 39:510–516.
3. Burn, P. 1988. Amphitropic proteins: a new class of membrane proteins. *Trends Biochem. Sci.* 13:79–83.
4. Tanaka, K., J. M. Caaveiro, and K. Tsumoto. 2015. Bidirectional transformation of a metamorphic protein between the water-soluble and transmembrane native states. *Biochemistry.* 54:6863–6866.
5. Lella, M., and R. Mahalakshmi. 2017. Metamorphic proteins: emergence of dual protein folds from one primary sequence. *Biochemistry.* 56:2971–2984.
6. García-Linares, S., E. Rivera-de-Torre, …, A. Martínez-del-Pozo. 2017. The metamorphic transformation of a water-soluble monomeric protein into an oligomeric transmembrane pore. *In* Advances in Biomembranes and Lipid Self-Assembly. A. Iglic, A. García-Sáez, and M. Rappolt, eds. Elsevier, pp. 51–97.
7. Alegre-Cebollada, J., M. Oñaderra, …, A. M. del Pozo. 2007. Sea anemone actinoporins: the transition from a folded soluble state to a functionally active membrane-bound oligomeric pore. *Curr. Protein Pept. Sci.* 8:558–572.
8. García-Ortega, L., J. Alegre-Cebollada, …, J. G. Gavilanes. 2011. The behavior of sea anemone actinoporins at the water-membrane interface. *Biochim. Biophys. Acta.* 1808:2275–2288.
9. Rivera-de-Torre, E., Á. Martínez-Del-Pozo, and J. E. Garb. 2018. Stichodactyla helianthus' de novo transcriptome assembly: discovery of a new actinoporin isoform. *Toxicon.* 150:105–114.

10. Leychenko, E., M. Isaeva, …, E. Kozlovskaya. 2018. Multigene family of pore-forming toxins from sea anemone Heteractis crispa. *Mar. Drugs.* 16:E183.
11. Anderluh, G., I. Krizaj, …, J. Pungercar. 1999. Equinatoxins, pore-forming proteins from the sea anemone Actinia equina, belong to a multigene family. *Toxicon.* 37:1391–1401.
12. Rojko, N., M. Dalla Serra, …, G. Anderluh. 2016. Pore formation by actinoporins, cytolysins from sea anemones. *Biochim. Biophys. Acta.* 1858:446–456.
13. Bellomio, A., K. Morante, …, J. M. González-Mañas. 2009. Purification, cloning and characterization of fragaceatoxin C, a novel actinoporin from the sea anemone Actinia fragacea. *Toxicon.* 54:869–880.
14. Athanasiadis, A., G. Anderluh, …, D. Turk. 2001. Crystal structure of the soluble form of equinatoxin II, a pore-forming toxin from the sea anemone Actinia equina. *Structure.* 9:341–346.
15. Hinds, M. G., W. Zhang, …, R. S. Norton. 2002. Solution structure of the eukaryotic pore-forming cytolysin equinatoxin II: implications for pore formation. *J. Mol. Biol.* 315:1219–1229.
16. Mancheño, J. M., J. Martín-Benito, …, J. A. Hermoso. 2003. Crystal and electron microscopy structures of sticholysin II actinoporin reveal insights into the mechanism of membrane pore formation. *Structure.* 11:1319–1328.
17. Mechaly, A. E., A. Bellomio, …, D. M. Guérin. 2011. Structural insights into the oligomerization and architecture of eukaryotic membrane pore-forming toxins. *Structure.* 19:181–191.
18. García-Linares, S., I. Castrillo, …, J. G. Gavilanes. 2013. Three-dimensional structure of the actinoporin sticholysin I. Influence of long-distance effects on protein function. *Arch. Biochem. Biophys.* 532:39–45.
19. Tanaka, K., J. M. Caaveiro, …, K. Tsumoto. 2015. Structural basis for self-assembly of a cytolytic pore lined by protein and lipid. *Nat. Commun.* 6:6337.
20. Malovrh, P., G. Viero, …, G. Anderluh. 2003. A novel mechanism of pore formation: membrane penetration by the N-terminal amphipathic region of equinatoxin. *J. Biol. Chem.* 278:22678–22685.
21. Gutiérrez-Aguirre, I., A. Barlič, …, J. M. González-Mañas. 2004. Membrane insertion of the N-terminal α-helix of equinatoxin II, a sea anemone cytolytic toxin. *Biochem. J.* 384:421–428.
22. Rojko, N., K. C. Kristan, …, G. Anderluh. 2013. Membrane damage by an α-helical pore-forming protein, equinatoxin II, proceeds through a succession of ordered steps. *J. Biol. Chem.* 288:23704–23715.
23. Antonini, V., V. Pérez-Barzaga, …, M. Tejuca. 2014. Functional characterization of sticholysin I and W111C mutant reveals the sequence of the actinoporin's pore assembly. *PLoS One.* 9:e110824.
24. Palacios-Ortega, J., S. García-Linares, …, J. P. Slotte. 2016. Regulation of sticholysin II-induced pore formation by lipid bilayer composition, phase state, and interfacial properties. *Langmuir.* 32:3476–3484.
25. Palacios-Ortega, J., S. García-Linares, …, J. P. Slotte. 2017. Differential effect of bilayer thickness on sticholysin activity. *Langmuir.* 33:11018–11027.
26. Rivera-de-Torre, E., J. Palacios-Ortega, …, Á. Martínez-Del-Pozo. 2017. One single salt bridge explains the different cytolytic activities shown by actinoporins sticholysin I and II from the venom of Stichodactyla helianthus. *Arch. Biochem. Biophys.* 636:79–89.
27. Shin, M. L., D. W. Michaels, and M. M. Mayer. 1979. Membrane damage by a toxin from the sea anemone Stoichactis helianthus. II. Effect of membrane lipid composition in a liposome system. *Biochim. Biophys. Acta.* 555:79–88.
28. Belmonte, G., C. Pederzolli, …, G. Menestrina. 1993. Pore formation by the sea anemone cytolysin equinatoxin II in red blood cells and model lipid membranes. *J. Membr. Biol.* 131:11–22.
29. Tejuca, M., M. D. Serra, …, G. Menestrina. 1996. Mechanism of membrane permeabilization by sticholysin I, a cytolysin isolated from the venom of the sea anemone Stichodactyla helianthus. *Biochemistry.* 35:14947–14957.
30. de los Ríos, V., J. M. Mancheño, …, J. G. Gavilanes. 1998. Mechanism of the leakage induced on lipid model membranes by the hemolytic protein sticholysin II from the sea anemone Stichodactyla helianthus. *Eur. J. Biochem.* 252:284–289.
31. Valcarcel, C. A., M. Dalla Serra, …, G. Menestrina. 2001. Effects of lipid composition on membrane permeabilization by sticholysin I and II, two cytolysins of the sea anemone Stichodactyla helianthus. *Biophys. J.* 80:2761–2774.
32. Martínez, D., A. Otero, …, E. Lissi. 2007. Effect of sphingomyelin and cholesterol on the interaction of St II with lipidic interfaces. *Toxicon.* 49:68–81.
33. Bakrač, B., and G. Anderluh. 2010. Molecular mechanism of sphingomyelin-specific membrane binding and pore formation by actinoporins. *Adv. Exp. Med. Biol.* 677:106–115.
34. García-Linares, S., J. Palacios-Ortega, …, J. P. Slotte. 2016. Toxin-induced pore formation is hindered by intermolecular hydrogen bonding in sphingomyelin bilayers. *Biochim. Biophys. Acta.* 1858:1189–1195.
35. García-Linares, S., E. Rivera-de-Torre, …, Á. Martínez-Del-Pozo. 2016. Differential effect of membrane composition on the pore-forming ability of four different sea anemone actinoporins. *Biochemistry.* 55:6630–6641.
36. Bernheimer, A. W., and L. S. Avigad. 1976. Properties of a toxin from the sea anemone Stoichacis helianthus, including specific binding to sphingomyelin. *Proc. Natl. Acad. Sci. USA.* 73:467–471.
37. Bakrač, B., I. Gutiérrez-Aguirre, …, G. Anderluh. 2008. Molecular determinants of sphingomyelin specificity of a eukaryotic pore-forming toxin. *J. Biol. Chem.* 283:18665–18677.
38. Maula, T., Y. J. Isaksson, …, J. P. Slotte. 2013. 2NH and 3OH are crucial structural requirements in sphingomyelin for sticholysin II binding and pore formation in bilayer membranes. *Biochim. Biophys. Acta.* 1828:1390–1395.
39. Varanda, W., and A. Finkelstein. 1980. Ion and nonelectrolyte permeability properties of channels formed in planar lipid bilayer membranes by the cytolytic toxin from the sea anemone, Stoichactis helianthus. *J. Membr. Biol.* 55:203–211.
40. Barlič, A., I. Gutiérrez-Aguirre, …, J. M. González-Mañas. 2004. Lipid phase coexistence favors membrane insertion of equinatoxin-II, a pore-forming toxin from Actinia equina. *J. Biol. Chem.* 279:34209–34216.
41. Alegre-Cebollada, J., I. Rodríguez-Crespo, …, A. M. del Pozo. 2006. Detergent-resistant membranes are platforms for actinoporin pore-forming activity on intact cells. *FEBS J.* 273:863–871.
42. Alegre-Cebollada, J., M. Cunietti, …, A. Martínez-del-Pozo. 2008. Calorimetric scrutiny of lipid binding by sticholysin II toxin mutants. *J. Mol. Biol.* 382:920–930.
43. Pedrera, L., M. L. Fanani, …, C. Álvarez. 2014. Sticholysin I-membrane interaction: an interplay between the presence of sphingomyelin and membrane fluidity. *Biochim. Biophys. Acta.* 1838:1752–1759.
44. Pedrera, L., A. B. Gomide, …, C. Álvarez. 2015. The presence of sterols favors sticholysin I-membrane association and pore formation regardless of their ability to form laterally segregated domains. *Langmuir.* 31:9911–9923.
45. Alm, I., S. García-Linares, …, J. P. Slotte. 2015. Cholesterol stimulates and ceramide inhibits sticholysin II-induced pore formation in complex bilayer membranes. *Biochim. Biophys. Acta.* 1848:925–931.
46. Wacklin, H. P., B. B. Bremec, …, R. S. Norton. 2016. Neutron reflection study of the interaction of the eukaryotic pore-forming actinoporin equinatoxin II with lipid membranes reveals intermediate states in pore formation. *Biochim. Biophys. Acta.* 1858:640–652.
47. Marchioretto, M., M. Podobnik, …, G. Anderluh. 2013. What planar lipid membranes tell us about the pore-forming activity of cholesterol-dependent cytolysins. *Biophys. Chem.* 182:64–70.

48. García-Linares, S., I. Alm, …, Á. Martínez-Del-Pozo. 2015. The effect of cholesterol on the long-range network of interactions established among sea anemone sticholysin II residues at the water-membrane interface. *Mar. Drugs.* 13:1647–1665.

49. Schön, P., A. J. García-Sáez, …, P. Schwille. 2008. Equinatoxin II permeabilizing activity depends on the presence of sphingomyelin and lipid phase coexistence. *Biophys. J.* 95:691–698.

50. Maček, P., M. Zecchini, …, G. Menestrina. 1997. Effect of membrane partitioned n-alcohols and fatty acids on pore-forming activity of a sea anemone toxin. *Eur. Biophys. J.* 25:155–162.

51. Niemelä, P., M. T. Hyvönen, and I. Vattulainen. 2004. Structure and dynamics of sphingomyelin bilayer: insight gained through systematic comparison to phosphatidylcholine. *Biophys. J.* 87:2976–2989.

52. Róg, T., and M. Pasenkiewicz-Gierula. 2006. Cholesterol-sphingomyelin interactions: a molecular dynamics simulation study. *Biophys. J.* 91:3756–3767.

53. Björkbom, A., T. Róg, …, J. P. Slotte. 2010. Effect of sphingomyelin headgroup size on molecular properties and interactions with cholesterol. *Biophys. J.* 99:3300–3308.

54. Endapally, S., D. Frias, …, A. Radhakrishnan. 2019. Molecular discrimination between two conformations of sphingomyelin in plasma membranes. *Cell.* 176:1040–1053.e17.

55. Térová, B., J. P. Slotte, and T. K. Nyholm. 2004. Miscibility of acyl-chain defined phosphatidylcholines with N-palmitoyl sphingomyelin in bilayer membranes. *Biochim. Biophys. Acta.* 1667:182–189.

56. Fischer, R. T., F. A. Stephenson, …, F. Schroeder. 1984. delta 5,7,9(11)-Cholestatrien-3 beta-ol: a fluorescent cholesterol analogue. *Chem. Phys. Lipids.* 36:1–14.

57. Alegre-Cebollada, J., G. Clementi, …, A. M. Pozo. 2007. Silent mutations at the 5′-end of the cDNA of actinoporins from the sea anemone Stichodactyla helianthus allow their heterologous overproduction in Escherichia coli. *J. Biotechnol.* 127:211–221.

58. García-Linares, S., T. Maula, …, Á. Martínez-Del-Pozo. 2016. Role of the tryptophan residues in the specific interaction of the sea anemone Stichodactyla helianthus's actinoporin sticholysin II with biological membranes. *Biochemistry.* 55:6406–6420.

59. Rouser, G., S. Fkeischer, and A. Yamamoto. 1970. Two dimensional then layer chromatographic separation of polar lipids and determination of phospholipids by phosphorus analysis of spots. *Lipids.* 5:494–496.

60. Gasset, M., A. Martínez del Pozo, …, J. G. Gavilanes. 1989. Study of the interaction between the antitumour protein α-sarcin and phospholipid vesicles. *Biochem. J.* 258:569–575.

61. Gasset, M., M. Oñaderra, …, J. G. Gavilanes. 1991. Acid phospholipid vesicles produce conformational changes on the antitumour protein α-sarcin. *Biochim. Biophys. Acta.* 1080:51–58.

62. Gasset, M., J. M. Mancheño, …, J. G. Gavilanes. 1995. Spectroscopic characterization of the alkylated α-sarcin cytotoxin: analysis of the structural requirements for the protein-lipid bilayer hydrophobic interaction. *Biochim. Biophys. Acta.* 1252:43–52.

63. Gasset, M., J. M. Mancheño, …, J. G. Gavilanes. 1995. Thermal unfolding of the cytotoxin alpha-sarcin: phospholipid binding induces destabilization of the protein structure. *Biochim. Biophys. Acta.* 1252:126–134.

64. de Antonio, C., A. Martínez del Pozo, …, J. G. Gavilanes. 2000. Assignment of the contribution of the tryptophan residues to the spectroscopic and functional properties of the ribotoxin α-sarcin. *Proteins.* 41:350–361.

65. Schroeder, F., G. Nemecz, …, T. E. Thompson. 1988. Fluorescence properties of cholestatrienol in phosphatidylcholine bilayer vesicles. *Biophys. Chem.* 32:57–72.

66. Wolber, P. K., and B. S. Hudson. 1979. An analytic solution to the Förster energy transfer problem in two dimensions. *Biophys. J.* 28:197–210.

67. Holt, A., R. F. de Almeida, …, J. A. Killian. 2008. Is there a preferential interaction between cholesterol and tryptophan residues in membrane proteins? *Biochemistry.* 47:2638–2649.

68. Lakowicz, J. R. 2006. Principles of Fluorescence Spectroscopy. Springer, New York.

69. Loura, L. M., A. Fedorov, and M. Prieto. 1996. Resonance energy transfer in a model system of membranes: application to gel and liquid crystalline phases. *Biophys. J.* 71:1823–1836.

70. Vos, W. L., R. B. Koehorst, …, M. A. Hemminga. 2005. Membrane-bound conformation of M13 major coat protein: a structure validation through FRET-derived constraints. *J. Biol. Chem.* 280:38522–38527.

71. Chen, R. F. 1967. Fluorescence quantum yields of tryptophan and tyrosine. *Anal. Lett.* 1:35–42.

72. Davenport, L., R. E. Dale, …, R. B. Cundall. 1985. Transverse location of the fluorescent probe 1,6-diphenyl-1,3,5-hexatriene in model lipid bilayer membrane systems by resonance excitation energy transfer. *Biochemistry.* 24:4097–4108.

73. Smaby, J. M., M. M. Momsen, …, R. E. Brown. 1997. Phosphatidylcholine acyl unsaturation modulates the decrease in interfacial elasticity induced by cholesterol. *Biophys. J.* 73:1492–1505.

74. Li, X. M., J. M. Smaby, …, R. E. Brown. 2000. Sphingomyelin interfacial behavior: the impact of changing acyl chain composition. *Biophys. J.* 78:1921–1931.

75. Hresko, R. C., I. P. Sugár, …, T. E. Thompson. 1987. The lateral distribution of pyrene-labeled sphingomyelin and glucosylceramide in phosphatidylcholine bilayers. *Biophys. J.* 51:725–733.

76. Hresko, R. C., I. P. Sugár, …, T. E. Thompson. 1986. Lateral distribution of a pyrene-labeled phosphatidylcholine in phosphatidylcholine bilayers: fluorescence phase and modulation study. *Biochemistry.* 25:3813–3823.

77. Jones, M. E., and B. R. Lentz. 1986. Phospholipid lateral organization in synthetic membranes as monitored by pyrene-labeled phospholipids: effects of temperature and prothrombin fragment 1 binding. *Biochemistry.* 25:567–574.

78. Kullberg, A., O. O. Ekholm, and J. P. Slotte. 2015. Miscibility of sphingomyelins and phosphatidylcholines in unsaturated phosphatidylcholine bilayers. *Biophys. J.* 109:1907–1916.

79. Ipsen, J. H., G. Karlström, …, M. J. Zuckermann. 1987. Phase equilibria in the phosphatidylcholine-cholesterol system. *Biochim. Biophys. Acta.* 905:162–172.

80. Nyholm, T. K., D. Lindroos, …, J. P. Slotte. 2011. Construction of a DOPC/PSM/cholesterol phase diagram based on the fluorescence properties of trans-parinaric acid. *Langmuir.* 27:8339–8350.

81. Wang, T. Y., and J. R. Silvius. 2003. Sphingolipid partitioning into ordered domains in cholesterol-free and cholesterol-containing lipid bilayers. *Biophys. J.* 84:367–378.

82. Björkqvist, Y. J., T. K. Nyholm, …, B. Ramstedt. 2005. Domain formation and stability in complex lipid bilayers as reported by cholestatrienol. *Biophys. J.* 88:4054–4063.

83. Koivusalo, M., J. Alvesalo, …, P. Somerharju. 2004. Partitioning of pyrene-labeled phospho- and sphingolipids between ordered and disordered bilayer domains. *Biophys. J.* 86:923–935.

84. Gasset, M., J. A. Killian, …, B. de Kruijff. 1988. Influence of cholesterol on gramicidin-induced HII phase formation in phosphatidylcholine model membranes. *Biochim. Biophys. Acta.* 939:79–88.

85. Schiffer, M., C. H. Chang, and F. J. Stevens. 1992. The functions of tryptophan residues in membrane proteins. *Protein Eng.* 5:213–214.

86. Dougherty, D. A. 1996. Cation-π interactions in chemistry and biology: a new view of benzene, Phe, Tyr, and Trp. *Science.* 271:163–168.

87. White, S. H., and W. C. Wimley. 1998. Hydrophobic interactions of peptides with membrane interfaces. *Biochim. Biophys. Acta.* 1376:339–352.

88. Lönnfors, M., J. P. Doux, …, J. P. Slotte. 2011. Sterols have higher affinity for sphingomyelin than for phosphatidylcholine bilayers even at equal acyl-chain order. *Biophys. J.* 100:2633–2641.

89. Slotte, J. P. 2016. The importance of hydrogen bonding in sphingomyelin's membrane interactions with co-lipids. *Biochim. Biophys. Acta.* 1858:304–310.

90. Yasuda, T., M. A. Al Sazzad, …, J. P. Slotte. 2016. The influence of hydrogen bonding on sphingomyelin/colipid interactions in bilayer membranes. *Biophys. J.* 110:431–440.

91. Castrillo, I., N. A. Araujo, …, M. Bruix. 2010. Specific interactions of sticholysin I with model membranes: an NMR study. *Proteins.* 78:1959–1970.

92. López-Castilla, A., F. Pazos, …, J. R. Pires. 2014. Solution NMR analysis of the interaction between the actinoporin sticholysin I and DHPC micelles–correlation with backbone dynamics. *Proteins.* 82:1022–1034.

93. Pettersen, E. F., T. D. Goddard, …, T. E. Ferrin. 2004. UCSF Chimera–a visualization system for exploratory research and analysis. *J. Comput. Chem.* 25:1605–1612.

Biophysical Journal, Volume *116*

Supplemental Information

Sticholysin, Sphingomyelin, and Cholesterol: A Closer Look at a Tripartite Interaction

Juan Palacios-Ortega, Sara García-Linares, Esperanza Rivera-de-Torre, José G. Gavilanes, Álvaro Martínez-del-Pozo, and J. Peter Slotte

Supplemental information

Sticholysin, Sphingomyelin, and Cholesterol: A Closer Look at a Tripartite Interaction.

Juan Palacios-Ortega[1,2], Sara García-Linares[1,3], Esperanza Rivera-de-Torre[1], José G. Gavilanes[1], Álvaro Martínez-del-Pozo[1]* and J. Peter Slotte[2]*

[1] Departamento de Bioquímica y Biología Molecular, Universidad Complutense, Madrid 28040, Spain

[2] Biochemistry, Faculty of Science and Engineering, Åbo Akademi University, 20500 Turku, Finland

[3] Present address: Cell Biology Department, Harvard Medical School, Boston, MA 02115, USA

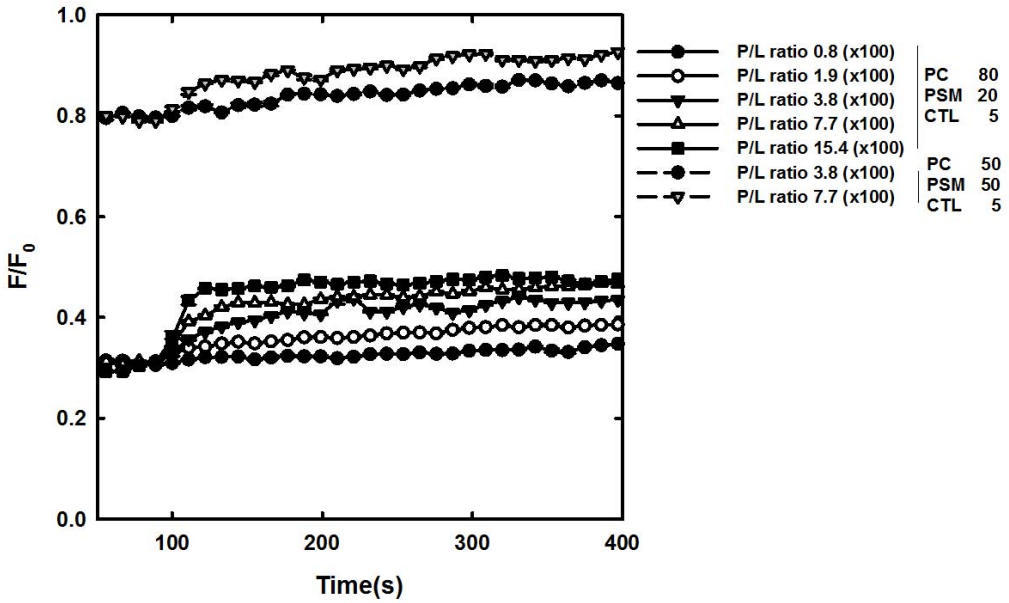

Figure S1. Representative F/F_0 traces of CTL emission as a function of time for different P/L ratios and membrane compositions. StnII was added at 100 s.

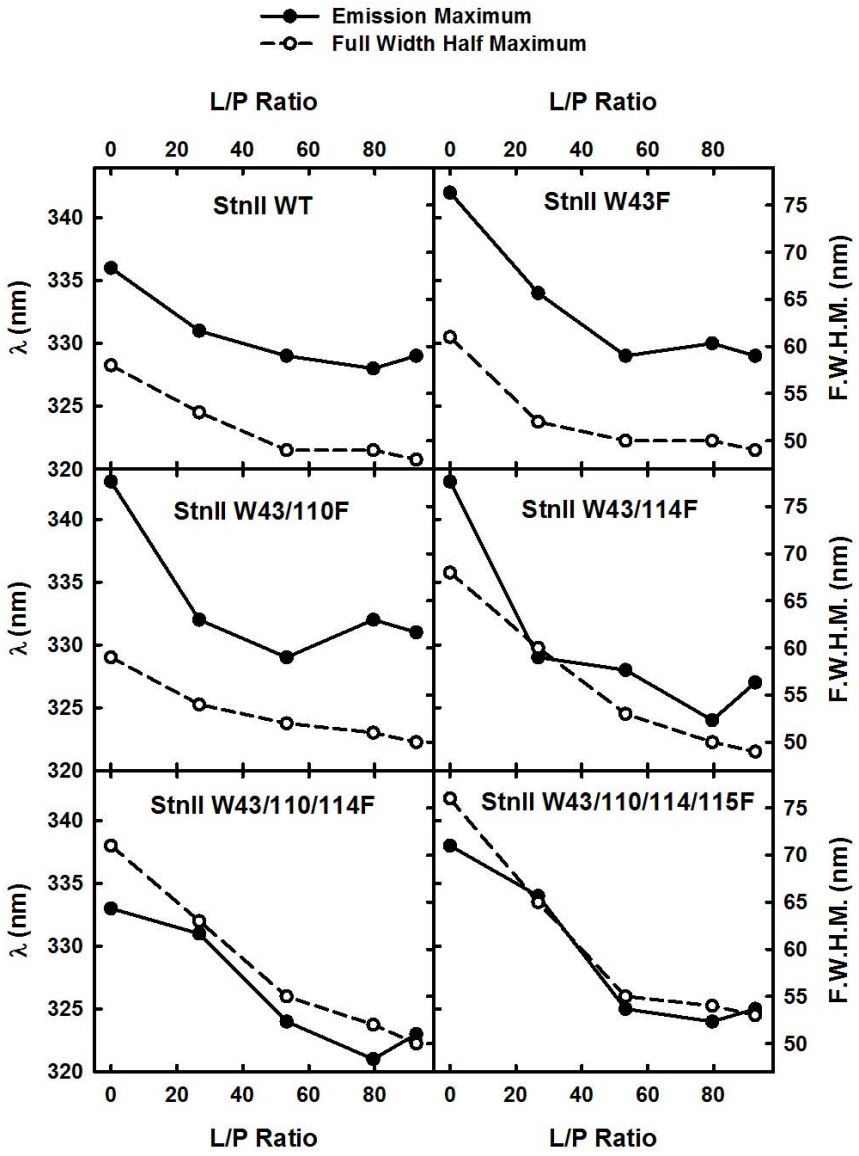

Figure S2. Graphs showing the change in the emission maximum (the right axis) and spectral width, measured as the full width at half of the maximum (FWHM, the left axis), for the emission spectra of StnII WT and the W mutants when titrated with vesicles composed of DOPC:eSM:Chol 1:1:1. The scales are the same for all panels.

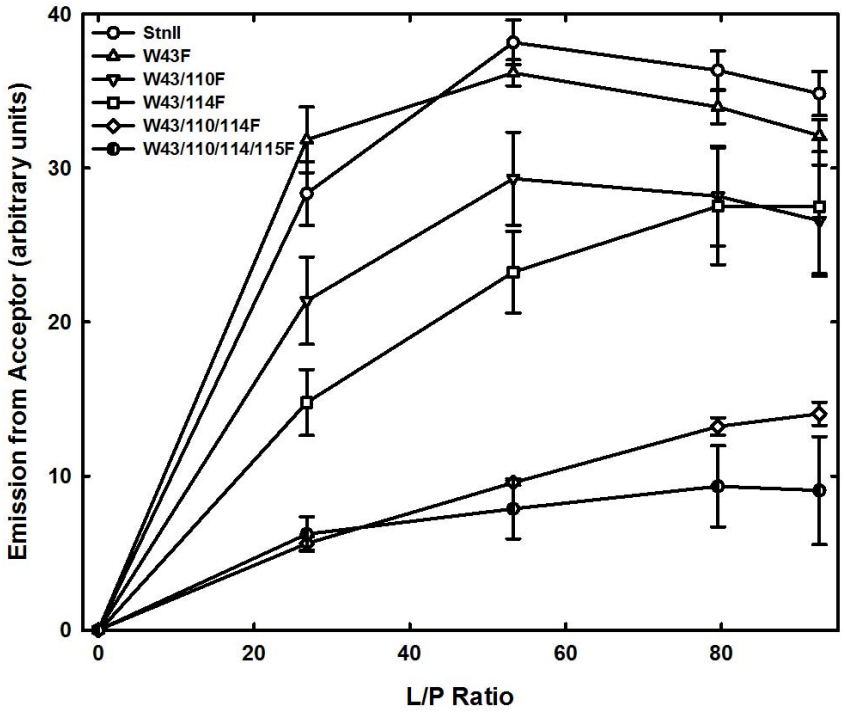

Figure S3. Representation of the energy transfer efficiency from StnII WT, or its Trp mutants studied, to CTL when titrated with DOPC:eSM:Chol:CTL (33:33:28:5) vesicles. The excitation wavelength employed was 260 nm. The spectra were recorded at 25 ºC. The protein concentration was 200 nM in all experiments shown. Fluorescence intensities were normalized to 1.0 for the maximum emission of StnII WT in buffer, in the absence of vesicles. Each value is the mean $\pm$ standard error on n=3.